Machine Learning for Thrombus Prediction in the Left Atrium Using CFD-Derived Hemodynamic Features

Júlio Gallinaro Maranho[1], João Lameu[1]

[1] Federal University of ABC, São Bernardo do Campo, Brazil

Abstract

Thrombus formation in the left atrium (LA) is a major clinical complication associated with atrial fibrillation (AF) and diastolic dysfunction (DD). This study proposes a machine learning pipeline to predict thrombogenic regions using hemodynamic indicators derived from patient-specific Computational Fluid Dynamics (CFD) simulations. A dataset comprising eight simulations from distinct clinical scenarios (Normal, DDI, DDII, DDIII) and two anatomical models was used. Four features—ECAP, OSI, RRT, and TAWSS—were extracted and used to train and evaluate eight classifiers. XGBoost was selected as the best model based on Dice Score, using cross-validation and statistical analysis (Friedman and Wilcoxon tests). The final model achieved a Dice Score of 0.772 ± 0.047 *on the test set. Evaluation across scenarios confirmed the model's robustness, and spatial visualizations enabled the identification of false positive and false negative regions. This approach enables high-throughput thrombus risk screening in patient-specific LA geometries and advances understanding of the hemodynamic correlates of thrombogenesis in DD and AF.*

1. Introduction

Atrial fibrillation (AF) is the most common cardiac arrhythmia worldwide and is a leading cause of cerebral ischemia, myocardial infarction, and venous thromboembolism [1,2]. AF can occur in conjunction with ventricular diastolic dysfunction (DD), a progressive condition characterized by abnormal mechanical function during the diastolic phase of the cardiac cycle [3]. Both AF and DD lead to alterations in atrial electromechanical function, resulting in inefficient blood pumping into the ventricles, atrial remodeling and enlargement, and increased blood stasis, which promotes thrombogenesis [4].

The risk of ischemic events in patients with AF is approximately five times higher than in healthy individuals [5]. Left atrial (LA) enlargement is frequently observed in patients with paroxysmal or persistent AF and DD, particularly in advanced stages. This enlargement reflects structural remodeling, including fibrosis, mechanical stress, and chronic dilation, which contribute to electrical instability [4]. These changes lead to abnormal atrial contraction patterns, increasing stiffness of the LA wall over time, and creating areas of blood stasis related to the generation of thrombi, particularly in the left atrial appendage (LAA) [6,7].

Computational Fluid Dynamics (CFD) has emerged as a valuable tool for assessing hemodynamic characteristics in AF [2,8], but no CFD studies have yet examined DD-specific hemodynamic conditions in the left atrium. CFD, or in silico hemodynamics, provides high-resolution spatiotemporal details, including velocity fields and derived parameters such as wall shear stress (WSS) and hemodynamic indicators (OSI, RRT, ECAP), which help identify thrombogenic zones. However, there is still no consensus on threshold values for stable clot formation [2,8].

To address this, coagulation cascade models have been proposed for the direct prediction of thrombus formation. These models solve advection-diffusion-reaction equations for biochemical species involved in clotting. Simplified versions (1–13 species) and artificially accelerated kinetics have been developed to reduce computational costs [9]. Few studies have applied these models to AF [10,11], and none to DD.

This study aims to develop and evaluate a machine learning framework capable of predicting thrombus-prone regions in the left atrium using hemodynamic indicators derived from patient-specific CFD simulations. By integrating simplified coagulation cascade modeling as ground truth, we investigate the discriminative power of four mechanical features (TAWSS, OSI, RRT, and ECAP) across multiple anatomical models and clinical scenarios, including atrial fibrillation and progressive stages of diastolic dysfunction. The goal is to support early thrombus risk stratification using high-throughput, interpretable models grounded in physics-based simulations, while significantly reducing the time required to generate reliable outputs.

2. Mathematical Modeling

2.1. Computational Fluid Dynamics

The Ansys CFD package was used in the CFD simulations. Five patient-specific 3D LA models were obtained from open dataset [12]. Hybrid volumetric meshes were generated. The 3D hemodynamic model was based on previous study [13]. The main characteristics are: laminar, isothermal, incompressible, transient/pulsatile flow, with non-Newtonian blood behavior (Carreau-Yasuda model). The boundary conditions were: Inlets – pulsatile velocity, adjusting the systolic/diastolic peak ratio (S/D) according to the pathophysiology scenario. Outlet: constant pressure of 8 mmHg at the mitral valve (MV), considering open with a fixed area along the cardiac cycle [6]. Walls: no-slip condition, due to the viscous blood, considering rigid-walls, representing the worst-case AF scenario (absence of atrial contraction). The effects of DD were simulated in four case studies were simulated by modifying the blood flow dynamics through the pulmonary veins, by changing the systolic/diastolic (S/D) peak ratio guided by clinical observations [14] and reflecting various stages of ventricular diastolic dysfunction, as described in Table 1. Five complete cardiac cycles were simulated, lasting 0.8 s, equivalent to a heart rate of 75 bpm and a cardiac output about 5L/min, using a time step of 1 x 10^{-3} s, and time-averaged values were obtained for the last two cardiac cycles.

Table 1. Description of the clinical scenarios simulated by CFD for each of the five LA models. All cases were considered to be under the worst scenario of AF (rigid walls and absence of atrial contraction).

Case	Description	S/D
0 (Normal)	Normal venous return	≈ 1.0
I (DDI	Altered relaxation pattern	≈ 2.1
II (DDII)	Pseudonormal condition	≈ 0.5
III (DDIII)	Restrictive pattern	≈ 0.2

The thrombosis-prone regions were assessed by well-established hemodynamic indicators based on WSS: the Time-Averaged Wall Shear Stress (TAWSS), with the thromboembolic risk classified as: TAWSS $<$ 0.1 Pa high risk, TAWSS $>$ 0.4 Pa low risk. The Oscillatory Shear Index (OSI), that describes the temporal change in the WSS direction relative to the predominant flow, the thromboembolic risk considered was: OSI $>$ 0.25 high risk and OSI $<$ 0.1 low risk. The Relative Residence Time (RRT), with a thromboembolic risk range of: RRT $>$ 25 high risk and RRT $<$ 10 low risk, and the Endothelial cell activation potential (ECAP) used to characterize thrombogenic susceptibility, with its thromboembolic risk range: ECAP $>$ 5 high risk and ECAP $<$ 0.5 low risk [6, 15, 16].

The simplified biochemical model for thrombogenesis (BMT) proposed by [9] was coupled to the 3D hemodynamic model. The BMT starts from the intrinsic path of coagulation, that can induce thrombus generation in the absence of tissue factor. Two cellular species - resting (RP) and activated platelets (AP), and one biochemical species - adenosine diphosphate (ADP), were considered in the numerical model by advective-diffusive-reactive equations, as described in previous study [13]. Also, the thrombus aggregation intensity marker, a volumetric estimation of stable clot, as proposed by [17] was integrated in the 3D hemodynamic model, providing a direct quantification of the thrombi, by defining a threshold of $\approx 10^{-7}[\text{cm}^{-3}]$ [13], based on the kinetic constants from [17] and [9], previously validated against $in\ vitro$ data of [17].

3. Model Selection

To identify the most effective classifier for thrombi prediction from hemodynamic indicators, we implemented a pipeline including preprocessing, model training, and evaluation using Dice Score as the metric due to its relevance in medical applications, especially in segmentation tasks [18].

Simulated data from multiple patient-specific geometries were saved in individual CSV files, each containing spatial coordinates (X, Y, Z), four hemodynamic features (ECAP, OSI, RRT, TAWSS), and a binary target label defined from the biochemical thrombogenesis model (BMT), using the thrombus aggregation intensity marker. Voxels above the threshold 10^{-7} cm^{-3} were labeled as thrombus-prone (1), while voxels below were labeled as non-thrombus (0).

Outliers in ECAP, RRT, and TAWSS were detected using the IQR method and corrected via nearest-neighbor interpolation. OSI required no correction. Although the hemodynamic indicators are not strictly independent, multicollinearity was evaluated using Variance Inflation Factor (VIF $<$ 7.07). These values indicate moderate correlation but not to a degree that would compromise the performance or stability of the classifiers.

Eight classifiers were evaluated: Logistic Regression, Ridge, Decision Tree, Random Forest, Extra Trees, HGBC, LightGBM, and XGBoost. Each integrated into a pipeline with Min-Max scaling. To ensure robust performance estimation and prevent data leakage, a 20-fold Group Shuffle Split strategy was adopted. This cross-validation approach guaranteed that all simulation data from a given case were kept within the same fold, avoiding fragmentation across training and validation sets.

Dice Scores obtained across the 20-fold cross-validation were compared using the Friedman test [19], which indicated statistically significant differences among classi-

fiers ($p < 0.001$). XGBoost achieved the highest average Dice Score (0.778 ± 0.048), followed closely by Histogram-Based Gradient Boosting Classifier (HGBC; 0.775 ± 0.050) and LightGBM (0.773 ± 0.052), showing a narrow performance gap among the top models.

To further investigate these differences, pairwise Wilcoxon signed-rank tests with Holm correction were performed. The resulting Critical Difference (CD) diagram (Figure 1) shows that XGBoost and Histogram-Based Gradient Boosting Classifier (HGBC) formed the top-performing clique, with no statistically significant difference between them ($p > 0.05$).

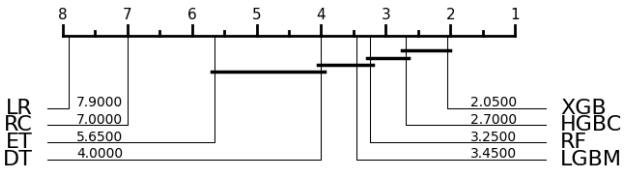

Figure 1. Critical Difference (CD) diagram generated from our classification results.

To complement this analysis, pairwise statistical comparisons were conducted to assess fold-wise consistency between XGBoost and HGBC, confirming the robustness of XGBoost across simulation scenarios. The application of a Wilcoxon signed-rank test corroborated a statistically significant superiority of XGBoost over HGBC ($p = 0.008$). These findings substantiate the choice of XGBoost as the final model for evaluation on the held-out test set.

4. Results

The final model, XGBoost, was retrained using the training dataset (LA01, LA02, LA04) and subsequently evaluated on the test set (LA05, LA09). All hemodynamic features were corrected for outliers using spatial interpolation and scaled via Min-Max normalization. Class imbalance ($\approx 1:7$) was addressed using class weighting.

On the full test set ($n = 281{,}125$ points), the model achieved a mean Dice Score of 0.772 ± 0.047, indicating high segmentation accuracy under challenging conditions involving heterogeneous geometries and hemodynamics.

Analysis on a per-mesh basis revealed consistent performance across multiple diastolic dysfunction stages and patient-specific LA anatomies (Table 2). LA09-DDII yielded the best result (Dice = 0.826), while LA05-DDIII exhibited the lowest score (Dice = 0.701), likely due to increased flow restriction and spatial complexity in that case.

A spatial visualization panel was created (Figure 2) to show the ground truth, predictions, and classification errors (TP, FP, FN).

Table 2. Dice score for each classification model evaluated under distinct CFD-simulated mesh scenarios.

Model	Scenario	Dice
LA05	DDI	0.703
LA05	DDII	0.758
LA05	DDIII	0.701
LA05	NormalFA	0.788
LA09	DDI	0.815
LA09	DDII	0.826
LA09	DDIII	0.785
LA09	NormalFA	0.795

5. Conclusion

This study proposed a machine learning framework to predict thrombus-prone regions in patient-specific left atrial geometries using CFD-derived hemodynamic features. By integrating simplified biochemical modeling as the ground truth, we demonstrated that mechanical indicators (TAWSS, OSI, RRT, ECAP) provide complementary information for classification.

Among eight evaluated classifiers, XGBoost achieved the highest and most consistent Dice Score, supported by statistical comparisons using the Friedman test and pairwise Wilcoxon signed-rank tests. This validates its robustness across multiple diastolic dysfunction scenarios.

The proposed approach enables high-throughput thrombus risk stratification and may assist in understanding the mechanistic links between atrial hemodynamics and thrombogenesis. Future developments should focus on designing machine learning models capable of replacing CFD simulations altogether, thereby reducing the time required to obtain thrombus risk indicators from several hours to just a few seconds, further supporting real-time clinical decision-making.

Acknowledgments

This study was financed in part by the Coordenação de Aperfeiçoamento de Pessoal de Nível Superior - Brasil (CAPES) - Finance Code 001. The authors thank the financial support by CNPq (National Council for Scientific and Technological Development, Process 405055/2023-4).

References

[1] Rahman F, Kwan GF, Benjamin EJ. Global epidemiology of atrial fibrillation. Nature Reviews Cardiology 2014; 11(11):639–654.

[2] Dueñas-Pamplona J, García JG, Sierra-Pallares J, Ferrera C, Agujetas R, Lopez-Minguez JR. A comprehensive comparison of various patient-specific cfd models of the left atrium

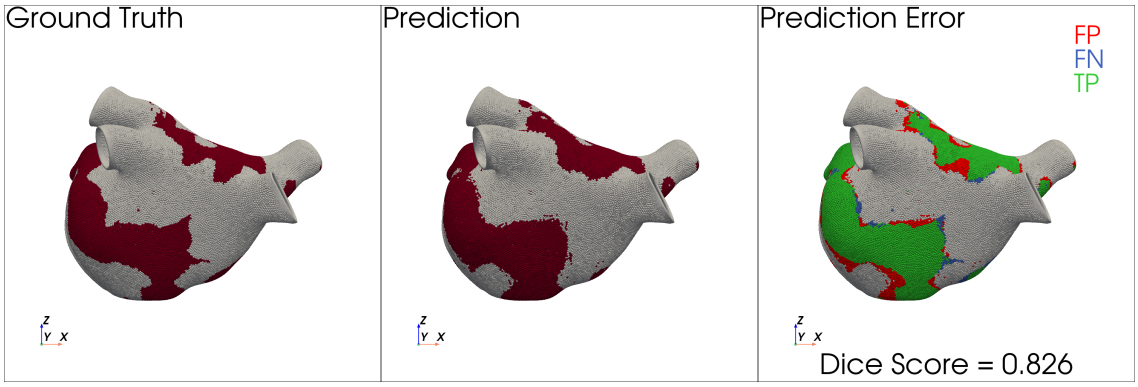

Figure 2. Comparison between ground truth and predicted segmentation of thrombus-prone regions in the left atrium (geometry LA09, Pseudonormal condition). Green areas represent true positives (TP), red areas false positives (FP), and blue areas false negatives (FN). The overall segmentation performance is summarized by a Dice Score of 0.826.

for atrial fibrillation patients. Computers in Biology and Medicine 2021;133:104423.

[3] Darwin L, Sembiring YE, Lefi A. Diastolic dysfunction and atrial fibrillation in coronary heart disease surgery: A literature review. International Journal of Surgery Open 2023; 55:100615.

[4] Park JH, Yang DH, Kim JH, Kim YR. Left atrium volume measured with multislice computed tomography as a prognostic predictor for atrial fibrillation catheter ablation outcomes. Journal of Clinical Medicine 2024;13(7):1859.

[5] Wang TJ, Massaro JM, Levy D, et al. A risk score for predicting stroke or death in individuals with new-onset atrial fibrillation in the community: the framingham heart study. JAMA 2003;290(8):1049–1056.

[6] Mill J, Agudelo V, Olivares AL, et al. Sensitivity analysis of in silico fluid simulations to predict thrombus formation after left atrial appendage occlusion. Mathematics 2021; 9(18):2304.

[7] Al-Saady N, Obel O, Camm A. Left atrial appendage: structure, function, and role in thromboembolism. Heart 1999;82(5):547–554.

[8] Masci A, Barone L, Dedè L, Fedele M, Tomasi C, Quarteroni A, Corsi C. The impact of left atrium appendage morphology on stroke risk assessment in atrial fibrillation: a computational fluid dynamics study. Frontiers in Physiology 2019;9:1938.

[9] Grande-Gutiérrez N, Alber M, Kahn AM, Burns JC, Mathew M, McCrindle BW, Marsden AL. Computational modeling of blood component transport related to coronary artery thrombosis in kawasaki disease. PLoS Computational Biology 2021;17(9):e1009331.

[10] Qureshi A, Darwish O, Dillon-Murphy D, Chubb H, Williams S, et al. Modelling left atrial flow and blood coagulation for risk of thrombus formation in atrial fibrillation. In 2020 Computing in Cardiology. IEEE, 2020; 1–4.

[11] Wang Y, Qiao YH, Mao Y, Jiang C, Fan J, Luo K. Numerical prediction of thrombosis risk in left atrium under atrial fibrillation. Math Biosci Eng 2020;17(3):2348–2360.

[12] Roney CH, Sim I, Yu J, Beach M, Mehta A, Alonso Solis-Lemus J, Kotadia I, Whitaker J, Corrado C, Razeghi O, et al. Predicting atrial fibrillation recurrence by combining population data and virtual cohorts of patient-specific left atrial models. Circulation Arrhythmia and Electrophysiology 2022;15(2):e010253.

[13] Lameu J, Sandoval I, Salinet J. Thrombogenesis and hemodynamics in left atrium under atrial fibrillation. In 2022 Computing in Cardiology (CinC), volume 498. IEEE, 2022; 1–4.

[14] Fernandez-Perez G, Duarte R, De la Calle MC, Calatayud J, González JS. Analysis of left ventricular diastolic function using magnetic resonance imaging. Radiologia English Edition 2012;54(4):295–305.

[15] Albors C, Mill J, Olivares AL, et al. Impact of occluder device configurations in in-silico left atrial hemodynamics for the analysis of device-related thrombus. PLOS Computational Biology 2024;20(9):e1011546.

[16] Gao Q, Lin H, Qian J, et al. A deep learning model for efficient end-to-end stratification of thrombotic risk in left atrial appendage. Engineering Applications of Artificial Intelligence 2023;126:107187.

[17] Taylor JO, Meyer RS, Deutsch S, Manning KB. Development of a computational model for macroscopic predictions of device-induced thrombosis. Biomechanics and modeling in mechanobiology 2016;15:1713–1731.

[18] Taha AA, Hanbury A. Metrics for evaluating 3d medical image segmentation: analysis, selection, and tool. BMC Medical Imaging 2015;15:1–28.

[19] Demšar J. Statistical comparisons of classifiers over multiple data sets. Journal of Machine Learning Research 2006; 7(Jan):1–30.

Address for correspondence:

Júlio Gallinaro Maranho
Biomedical Engineering, Center for Engineering, Modeling and Applied Social Sciences (CECS), Federal University of ABC
Alameda da Universidade, s/n, São Bernardo do Campo, Brazil
julio.gallinaro@ufabc.edu.br